Journal of Molecular Structure 1286 (2023) 135536

Contents lists available at ScienceDirect

Journal of Molecular Structure

journal homepage: www.elsevier.com/locate/molstr

Synthesis, crystal structure, physicochemical of new (±)-2,7-dimethoxy-3-(4-metho-xyphenyl)-3-methylchroman-4-one: DFT, Hirshfeld, optical and TD-DFT/DFT analysis

Nawaf Al-Maharik [a,b,*], Malak Daqqa [a], Abeer AlObaid [c], Abdelkader Zarrouk [d], Ismail Warad [a,*]

[a] Department of Chemistry, Science College, An-Najah National University, Nablus P.O. Box 7, Palestine
[b] School of Chemistry, Biomedical Sciences Research Complex, University of St Andrews, North Haugh, St Andrews, Fife KY16 9ST, United Kingdom
[c] Department of Chemistry, College of Science, King Saud University, P.O. Box 2455, Riyadh 11451, Saudi Arabia
[d] Laboratory of Materials, Nanotechnology and Environment, Mohammed V University in Rabat, Faculty of Sciences, Av. Ibn Battuta, PO B.P. 1014 Rabat, Morocco

ARTICLE INFO

Keywords:
Chroman-4-one
XRD-crystal
DFT-calculations
HSA
Optical

ABSTRACT

In a one-pot procedure, the novel 2,7-dimethoxy-3-(4-methoxyphenyl)-3-methylchroman-4-one was synthesized in high yield as a racemic combination by reacting 7,4′-dimethoxyisoflavone with NaOMe and iodomethane under inert atmosphere. NMR, CHN-EA, FT-IR, UV–vis, and XRD-crystal examinations were used to identify the target chemical. DFT-structural optimization and XRD were consistent. XRD investigation revealed that the molecule generated a number of C_{Me}-H·····O and C_{ph}-H·····O short interactions, resulting in the formation of two distinct types of synthons. The experimental XRD-packing data matched the values of molecular electronic potential (MEP), MAC/NBA, and Hirshfeld surface (HSA). The observed optical energy calculated from Tauc's relation was compared to the HOMO/LUMO and density of state (DOS) computations. Tauc's observed optical energy relationship was compared to its DOS and HOMO/LUMO theoretical values.

1. Introduction

Isoflavonoids are an important subclass of plant-derived flavonoids that are mostly found in the Leguminosae subfamily Papilionoideae [1]. They function as phytoalexins, which plants create in response to stress or pathogen attack [2,3]. Soybeans contain more isoflavonoids than any other leguminous crop, making them an important dietary source of these chemical groups [4]. Isoflavonoids are often referred to as phytoestrogens due to the fact that they have the same size and structure as human estrogens and can thus bind to both estrogen and estrogen receptors [5]. Scientists' interest in isoflavones has grown in recent years due to its possible health benefits, as evidenced by the growing number of nutritional health products containing isoflavonoids on the market [6]. Isoflavonoids have a wide range of biological effects, including antioxidant [1,7,8], anticarcinogenic [9,10], and antiproliferative activity [11], as well as the ability to prevent osteoporosis and lower the risk of cardiovascular disease [12]. They are sometimes referred to as dietary antioxidants, which are compounds that may protect against oxidative stress associated with inflammation as well as the risk of macromolecule damage caused by free radicals and related oxygen- and nitrogen-based oxidizing agents [13].

As part of our team's ongoing work to prepare heterocyclic compounds with nitrogen, sulfur, and oxygen atoms as well as their transition metal complexes for structural, catalytic, anticorrosion, and therapeutic applications [14–16]. Herein, we report the tandem reaction of 7,4′-dimethoxyisoflavone with NaOMe and iodomethane, which yields 2,7-dimethoxy-3-(4-methoxyphenyl)−3-methylchroman-4-one. The molecule's structure was determined using XRD-single crystal, NMR, UV–vis, FT-IR, and the B3LYP/DFT calculation. Furthermore, HOMO/LUMO and DOS were used to theoretically and experimentally establish direct optical activity using Tauc's relation.

2. Experimental

2.1. Materials, measurements, and computations details

The chemicals were purchased from Sigma-Aldrich and used without further purification. The IR was recorded in solid state in the range of 750–4000 cm^{-1} using a Shimadzu FTIR-8010M spectrometer. The ^{1}H and $^{13}CNMR$ spectra were acquired in $CDCl_3$ using a Jeol GSX WB

* Corresponding authors at: Department of Chemistry, Science College, An-Najah National University, Nablus P.O. Box 7, Palestine.
E-mail addresses: n.maharik@najah.edu (N. Al-Maharik), warad@najah.edu (I. Warad).

https://doi.org/10.1016/j.molstruc.2023.135536
Received 26 January 2023; Received in revised form 26 March 2023; Accepted 8 April 2023
Available online 9 April 2023

Table 1
Compound **2** structure refinement details.

Chemical formula	$C_{19}H_{20}O_5$
M_r	328.35
Crystal system	Triclinic
space group	*P*
Z	*2*
D_c *(mg/m^3)*	*1.333*
Color	*colorless*
Crystal description	prism
Temperature (K)	173
Limiting indices	$-7\leq h \leq 7$, $-12\leq k \leq 12$, $-14\leq l \leq 12$
Θ range (°)	3.72–67.68
Θ_{max} (°)	68.32
a, b, c (Å)	6.6670 (3), 10.5319 (5), 11.8825 (5)
GOF on F^2	1.032
F(000)	348
α, β, γ (°)	88.104 (4), 88.197 (4), 78.960 (4)
V (Å^3)	818.19 (6)
Radiation type	Cu-*K*α
μ (mm^{-1})	0.79
Crystal size (mm)	0.17 × 0.1 × 0.05
Absorption correction	CrysAlis PRO 1.171.40.14a (Rigaku Oxford Diffraction, 2018) Empirical absorption correction using spherical harmonics, implemented in SCALE3 ABSPACK scaling algorithm.
Diffractometer	Rigaku XtaLAB P100K
T_{min}, T_{max}	0.780, 1.000
No. of measured, independent and observed [$I > 2\sigma(I)$] reflections	7226, 2901, 2683
R_{int}	0.018
$(\sin\theta/\lambda)_{max}$ (Å^{-1})	0.603
$R[F^2 > 2\sigma(F^2)]$, $wR(F^2)$, *S*	0.041, 0.117, 1.09
$\Delta\rho_{max}$, $\Delta\rho_{min}$ (e Å^{-3})	0.24, −0.30

spectrometer at 400 MHz. The Gaussian09W program was utilized for the gaseous state DFT calculations at DFT/B3LYP/6-311G (d,p) [17]. The HSA calculation was performed using Crystal Explorer 3.1 software [18].

2.2. Synthesis of (±)−2,7-dimethoxy-3-(4-methoxyphenyl)−3-methylchroman-4-one

Under a nitrogen atmosphere, sodium methoxide (0.27 g, 5.00 mmol) was added to a solution of 7,4′-dimethoxyisoflavone **1** (1.41 g, 5.00 mmol) in dry DMF (20 mL). After 4 h of stirring at room temperature, iodomethane (0.47 mL, 7.55 mmol) was added in one portion, and the mixture was stirred for a further 12 h. The solution was poured into water (100 mL), and the precipitate was filtered and submitted to flash silica gel column chromatography (CH_2Cl_2/EtOAc 9:1 to 8:2) to offer 1.34 g (85%) of compound **2** as a white solid; ^{1}H NMR ($CDCl_3$, 400 MHz) δ 7.93 (d, J = 8.8 Hz, 1H, H-5), 7.37 (d, 8.8 Hz, 2H, H-2′,6′), 6.83 (d, J = 8.8 Hz, 2H, H-3′,5′), 6.66 (dd, J = 8.8, 2.4 Hz, 1H, H-6), 6.49 (d, J = 2.4 Hz, 1H, H-8), 5.04 (s, 1H, H-2), 3.87 (s, 3H, 7OCH$_3$–), 3.79 (s, 3H, 4′OCH$_3$–), 3.57 (s, 3H, 2OCH$_3$–), 1.67 (s, 3H, 3-C-CH$_3$).^{13}C NMR ($CDCl_3$, 400 MHz) δ 193.9 (C-4), 166.05 (C-7), 159.09 (C-4′), 158.56 (C-8), 129.83 (C-2′,6′), 129.61 (C-1′), 129.45 (C-5), 114,53 (C-4a), 113.30 (C-3′,5′), 110.27 (C-2), 108.66 (C-6), 101.20 (C-8), 57.66 (7-O-CH$_3$), 55.66 (4′-O-CH$_3$), 55.14 (2-O-CH$_3$), 53.09 (C-3), 20.70 (CH$_3$).

2.3. XRD-analysis

XRD-crystal data of isoflavanone **2** were recorded at 173 °K by means of the CrysalisPro software [19] on a Gemini kappa-geometry diffractometer (Rigaku XtaLAB P100K Rigaku) equipped with an Atlas CCD detector and using Mo radiation (λ= 0.71073 Å). The structure was solved with SHELXT [20]. The crystal data and structure refinement parameters of the free ligand are illustrated in Table 1.

3. Results and discussion

3.1. Synthesis of (±)−2,7-dimethoxy-3-(4-methoxyphenyl)−3-methylchroman-4-one 2

2,7-dimethoxy-3-(4-metho-xyphenyl)−3-methylchroman-4-one **2** was synthesized in a one-pot procedure by reacting 7,4′-dimethoxyisoflavone **1** with sodium methoxide in dry DMF under nitrogen atmosphere, followed by the addition of iodomethane, as shown in Scheme 1. Using 2D NMR and IR, as well as XRD crystallography, the structure of isoflavanones **2** was established. Isoflavanone **2** was determined to be a racemic combination using HPLC with a chiral column.

3.2. X-ray and DFT analysis

To confirm the 3D-structure of the 2,7-dimethoxy-3-(4-methoxyphenyl)−3-methylchroman-4-one, XRD and DFT have been performed, as seen in Fig. 1. Fig. 1a depicts XRD-ORTEP, whereas Fig. 1b depicts DFT for the molecular structure. The desired compound was crystallized in triclinic, space group P, with the following lattice parameters: a = 6.6670 (3), b = 10.5319 (5), c = 11.8825 (5) Å, α= 88.104 (4), β = 88.197 (4), and γ = 78.960 (2)°. The XRD outcomes reflected the formation of (∓)- 2,7-dimethoxy-3-(4-methoxyphenyl)−3-methylchroman-4-one with racemic centers. Table 2 and Fig. 1 demonstrate that the DFT-optimized structural parameters, including bond lengths and angles, correlate extremely well with the XRD data. XRD/DFT-bond lengths (Fig. 1b) with R^2 = 0.984 (Fig. 1c) and XRD/DFT-angles (Fig. 1d) with R^2 = 0.984 were in excellent agreement as indicated Fig. 1f. This observation verified the DFT-validity theory's ability to identify such structural properties, especially in organic compounds.

3.3. XRD-packing and HSA investigation

Several non-classical C—H·····O interactions add up to define the structure of 2,7-dimethoxy-3-(4-methoxyphenyl)−3-methylchroman-4-one **2**. The formation of two distinct types of new synthons is the result of short interactions between C_{Me}-H·····O and C_{ph}-H·····O, which are crucial for the structural stability of compounds [21–23]. The first synthon is of S9 type and generated via a 2-D hydrogen-bonded network, with two synthons per molecule constructed through nonclassical C_{ph}-H·····$O_{carbonyl}$ and C_{ph}-H····· $O_{chroman}$ interactions with 2.642 and 2.497 bond length and receptivity (Fig. 2a). The second synthon was of the S14 2-D type, one per molecule, formed via 2C_{ph}-H·····O_{Me} interactions with 2.433 Å (Fig. 2b). 1-D chain C_{Me}-H·····O with 2.537 Å, of which two bonds per molecule contribute to the self-assembly mode of interaction, as seen in Fig. 2c. Such non-classical and non-covalent [H·····O] interactions, together with associated synthons, were critical for 3D-crystal packing mode stability.

HSA calculation was performed using the original CIF file to support the 3D-XRD molecular interactions in the crystal lattice of 2,7-dimethoxy-3-(4-metho-xyphenyl)−3-methylchroman-4-one [24–28].

The presence of several polar atoms, electrostatic functional groups, and four main big-red points on the molecule surface was reflected in the molecular structure (Fig. 3a), d_{norm} (Fig. 3b), and shape index (Fig. 3c), resulting in the formation of four non-covalent hydrogen bonds of type C—H·····O interactions. As revealed by the XRD data, the presence of this number of spots on the calculated surface of the isoflavanones **2** suggested the possibility of binding *via* four valuable [H·····O] H-bonds. Furthermore, as illustrated in Fig. 3d, the 2D-FP computations verified the presence of intermolecular interactions in the dependent: H·····H (52.3%)>C·····H(11.1%)>*O*·····H(10.1%).

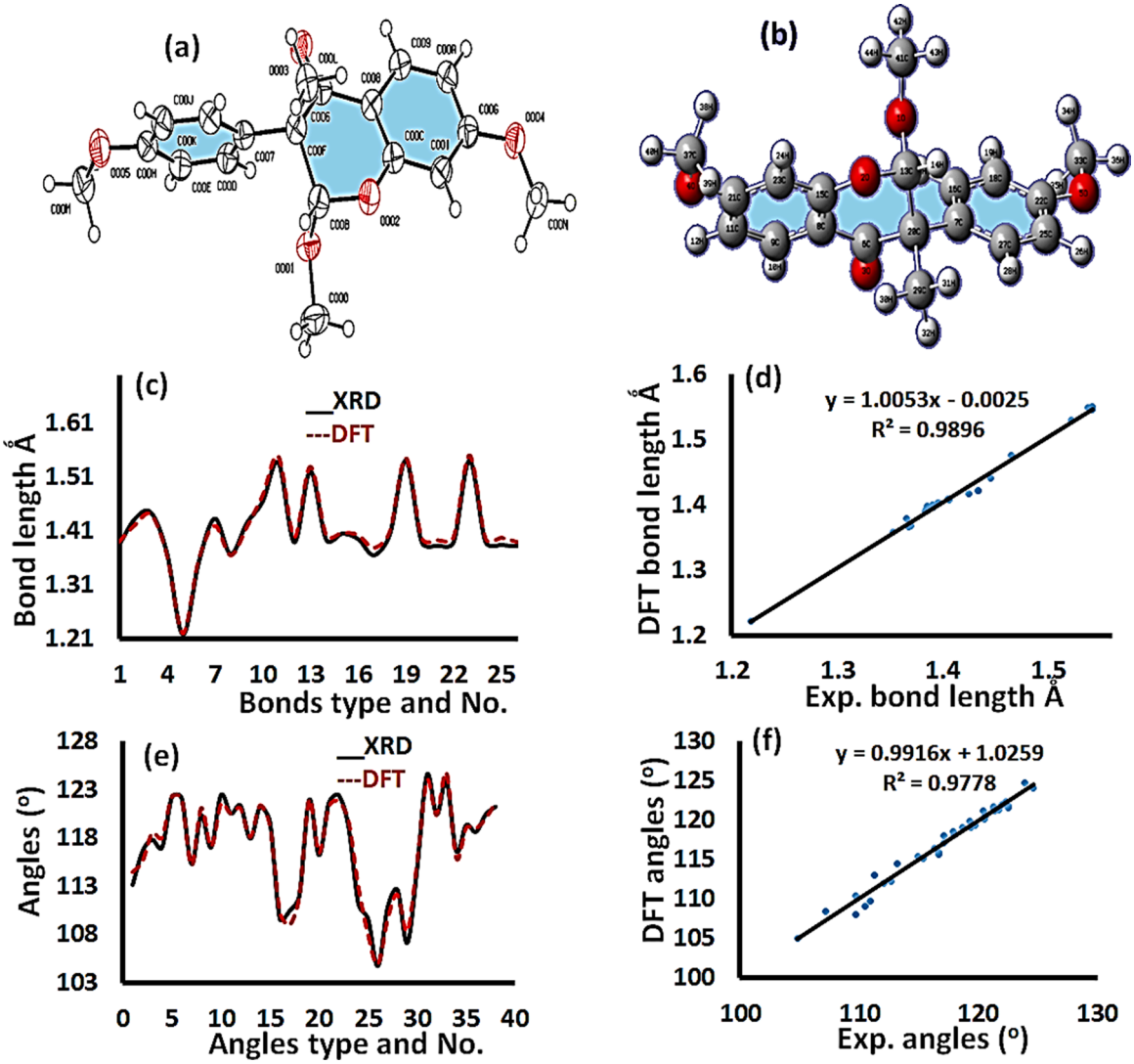

Fig. 1. (a) XRD, (b) DFT-optimization structure, (c) XRD/DFT-histogram of bond lengths, (d) XRD/DFT-graphical correlation for bond lengths (e), XRD/DFT-histogram of angles, and (f) XRD/DFT-graphical correlation for angles.

Table 2
All DFT/XRD bond angles and angles.

Bond No.	Bond type		XRD	DFT	Angle No.	Angle type			XRD	DFT
1	O001	C00B	1.385(2)	1.3915	1	C00B	O001	C00O	113.2(1)	114.56
2	O001	C00O	1.434(2)	1.4230	2	C00B	O002	C00C	116.67(9)	115.68
3	O002	C00B	1.445(2)	1.4422	3	C00G	O004	C00N	117.9(1)	118.61
4	O002	C00C	1.370(1)	1.3676	4	C00H	O005	C00M	117.1(1)	118.11
5	O003	C006	1.218(2)	1.2216	5	O003	C006	C008	122.3(1)	122.37
6	O004	C00G	1.353(1)	1.3581	6	O003	C006	C00F	122.2(1)	122.2
7	O004	C00N	1.434(2)	1.4216	7	C008	C006	C00F	115.4(1)	115.23
8	O005	C00H	1.368(2)	1.3667	8	C00D	C007	C00F	120.4(1)	121.17
9	O005	C00M	1.425(2)	1.4183	9	C00D	C007	C00K	117.1(1)	117.17
10	C006	C008	1.465(2)	1.4768	10	C00F	C007	C00K	122.5(1)	121.6
11	C006	C00F	1.538(2)	1.5497	11	C006	C008	C009	120.6(1)	120.62
12	C007	C00D	1.390(2)	1.4004	12	C006	C008	C00C	121.4(1)	121.18
13	C007	C00F	1.522(2)	1.5309	13	C009	C008	C00C	118.0(1)	118.17
14	C007	C00K	1.395(2)	1.4035	14	C008	C009	C00A	121.3(1)	121.46
15	C008	C009	1.406(2)	1.4079	15	C009	C00A	C00G	119.7(1)	119.43
16	C008	C00C	1.396(2)	1.4041	16	O001	C00B	O002	109.7(1)	110.41
17	C009	C00A	1.366(2)	1.3801	17	O001	C00B	C00F	110.5(1)	109.06
18	C00A	C00G	1.405(2)	1.4104	18	O002	C00B	C00F	112.1(1)	112.03
19	C00B	C00F	1.542(2)	1.5470	19	O002	C00C	C008	122.0(1)	122.07
20	C00C	C00I	1.390(2)	1.3978	20	O002	C00C	C00I	116.3(1)	116.52
21	C00D	C00E	1.384(2)	1.3944	21	C008	C00C	C00I	121.7(1)	121.39
22	C00E	C00H	1.390(2)	1.3996	22	C007	C00D	C00E	122.5(1)	121.93
23	C00F	C00L	1.542(2)	1.5518	23	C00D	C00E	C00H	119.3(1)	119.85
24	C00G	C00I	1.391(2)	1.3973	24	C006	C00F	C007	111.3(1)	113.09
25	C00H	C00J	1.385(2)	1.3988	25	C006	C00F	C00B	109.7(1)	108.11
26	C00J	C00K	1.383(2)	1.3908	26	C006	C00F	C00L	104.8(1)	105.01
					27	C007	C00F	C00B	110.9(1)	109.73
					28	C007	C00F	C00L	112.7(1)	112.22
					29	C00B	C00F	C00L	107.2(1)	108.44
					30	O004	C00G	C00A	114.9(1)	115.46
					31	O004	C00G	C00I	124.6(1)	124.06
					32	C00A	C00G	C00I	120.5(1)	120.48
					33	O005	C00H	C00E	123.9(1)	124.82
					34	O005	C00H	C00J	116.7(1)	116.02
					35	C00E	C00H	C00J	119.4(1)	119.16
					36	C00C	C00I	C00G	118.7(1)	119.06
					37	C00H	C00J	C00K	120.5(1)	120.15
					38	C007	C00K	C00J	121.3(1)	121.74

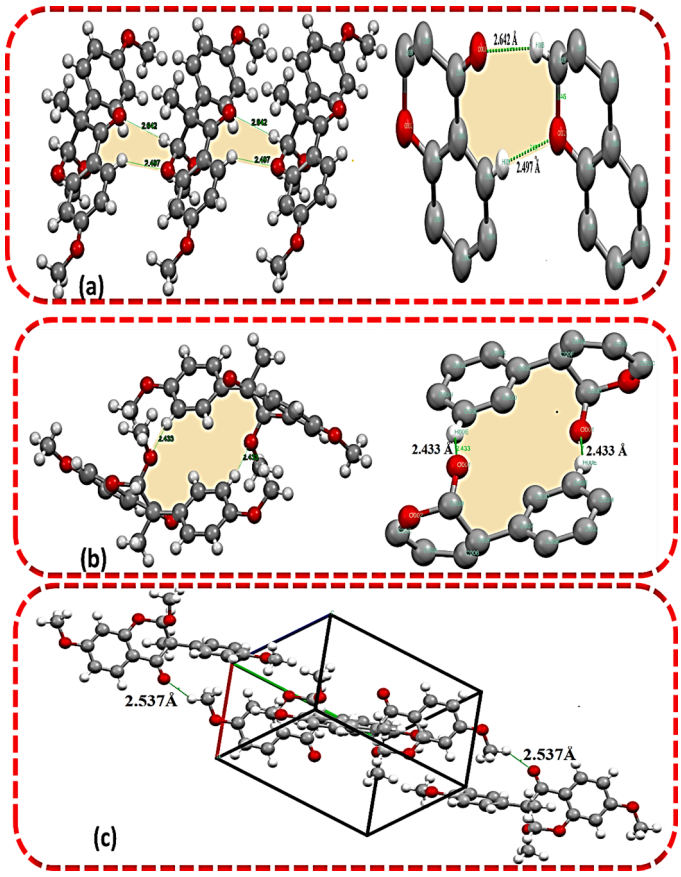

Fig. 2. (a) 2D-S9, and (b) 2D-S14 C_{Ph}-H⋯O synthons, and (c) 1D linear C_{Me}-H⋯O interactions.

3.4. MEP, MAC and NPA analysis

The DFT/B3LYP approach at 6–311G(d,p) MEP offered useful electrostatic information about all of the atoms in the molecule's backbone; as a result, some of the functional groups were categorized as electrophilic/nucleophilic or neutral by color indication as follows: blue (electrophilic) > cyan > green (neutrophilic) > yellow > orange>red (nucleophilic) (Fig. 4a). The MEP also indicates four O (the highest being O of carbonyl) and several C's as nucleophilic sites, whereas all H's and a few C's are electrophilic or neutral (Fig. 4b). As illustrated in Fig. 4c and Table 3, the MAC/NPA charge calculations aid in determining the number of atoms in a molecule.

In general, NBA charges are greater than MAC charges; nevertheless, all O atoms are negatively charged, with the O of carbonyl having the greatest value. The majority of carbons have a low negative charge [24, 29], meanwhile, all of the H's have a positive charge, with the H's Me having the largest positive value. Because certain H's in Me and pH are electrostatic and the O atoms are highly nucleophilic, MEP and MAC/NPA simulations suggest the probability of CH⋯O H-bonding formation.

3.5. ^{1}H and ^{13}C NMR investigations

Compound 2′s structural scaffold was established by ^{1}H and ^{13}C, and 2D NMR analysis (Fig. 5), where the experimental ^{1}HNMR was compared to the theoretical one in $CDCl_3$ as shown in Figs. 5a and 5b. The ^{1}HNMR spectra revealed one Me, three OMe, and one CH proton in the aliphatic area of 1–5 ppm, whereas aromatic protons were detected in the 6.5–8.5 ppm range. As predicted, the O_2C—H acetal proton is found as a singlet with a high chemical shift of 5.0 ppm. All of the protons were directly related to their expected chemical shifts, as shown in Fig. 5. In terms of theoretical ^{1}HNMR measurements, all of the protons' chemical shifts exhibited a strong correlation with their experimental counterparts' chemical shifts, with only minor deviations in certain situations (Fig. 5b). In general, the high graphical correlation value (0.99) indicates an exceptional degree of congruence between the two data shown in Fig. 5c.

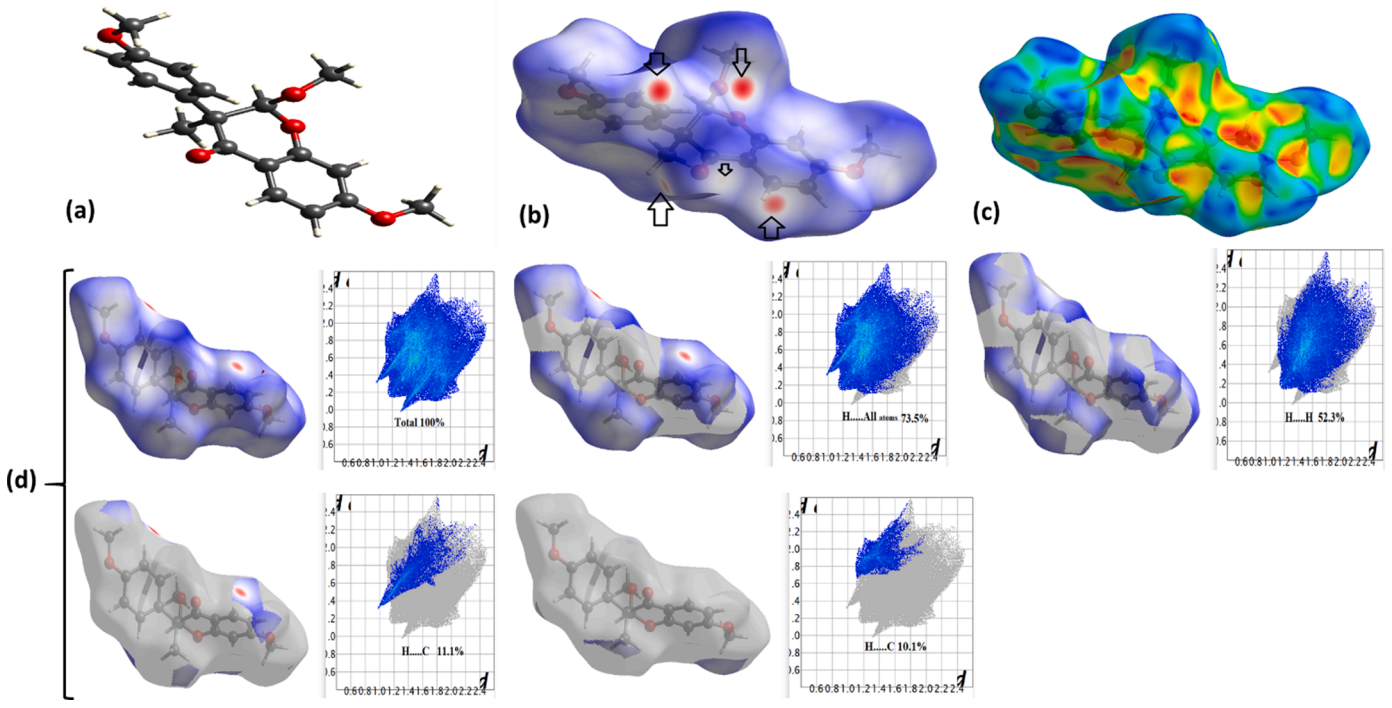

Fig. 3. HSA computation: (a) Molecular structure, (b) d_{norm}, (c) Shape index, and (d) 2D-FP analysis.

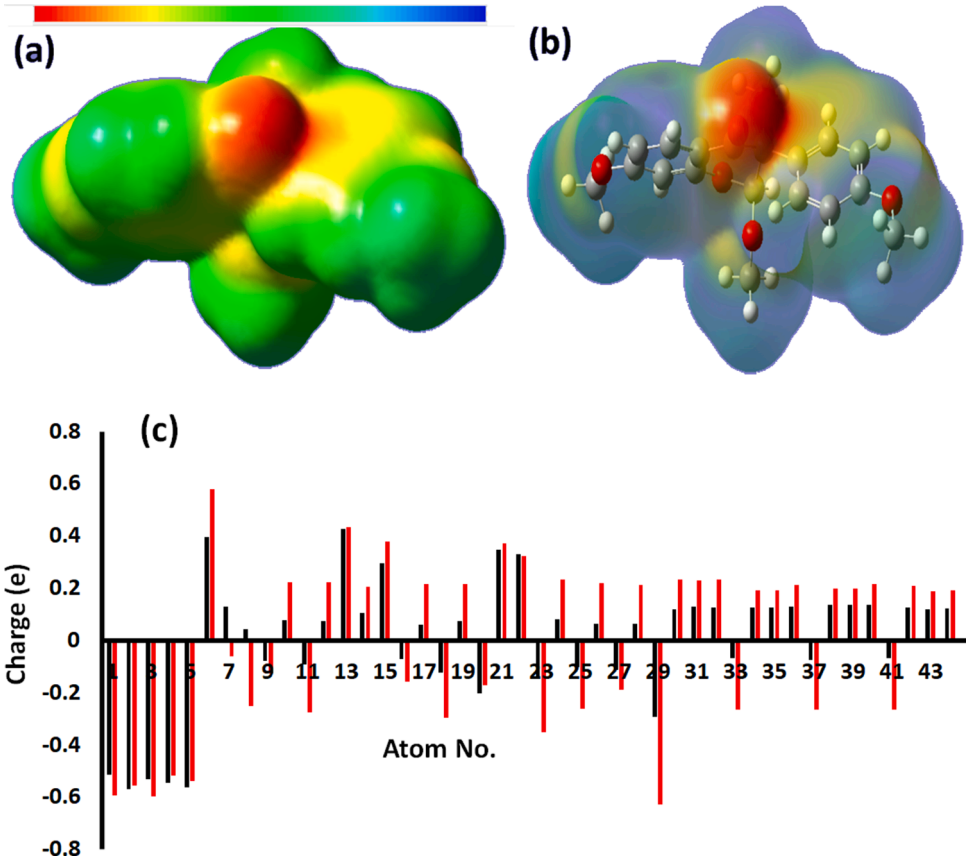

Fig. 4. (a) Rigid MEP, (b) obvious Map, and (c) MAC/NBA charge.

Table 3
MAC and NBA charge.

No.	Atom	MAC	NBA	No.	Atom	MAC	NBA
1	O	−0.5127	−0.59261	23	C	−0.14161	−0.34884
2	O	−0.56692	−0.55428	24	H	0.083161	0.23232
3	O	−0.53175	−0.597	25	C	−0.10226	−0.25971
4	O	−0.54501	−0.51753	26	H	0.065407	0.21882
5	O	−0.56054	−0.53818	27	C	−0.11233	−0.18839
6	C	0.395199	0.57871	28	H	0.065123	0.21215
7	C	0.132004	−0.06087	29	C	−0.29114	−0.62572
8	C	0.043965	−0.25146	30	H	0.121458	0.23504
9	C	−0.07667	−0.12469	31	H	0.130959	0.23012
10	H	0.07724	0.22269	32	H	0.1285	0.23533
11	C	−0.09058	−0.27357	33	C	−0.06783	−0.26386
12	H	0.075745	0.22433	34	H	0.12643	0.19392
13	C	0.42866	0.43546	35	H	0.12835	0.19196
14	H	0.104459	0.20664	36	H	0.128796	0.21343
15	C	0.296665	0.37767	37	C	−0.07223	−0.26505
16	C	−0.06966	−0.15814	38	H	0.135574	0.19834
17	H	0.061454	0.21696	39	H	0.136686	0.1979
18	C	−0.12058	−0.29343	40	H	0.137423	0.21762
19	H	0.073436	0.21793	41	C	−0.0677	−0.26282
20	C	−0.20276	−0.16947	42	H	0.128348	0.21076
21	C	0.348434	0.37164	43	H	0.12153	0.18964
22	C	0.332425	0.32243	44	H	0.124819	0.19381

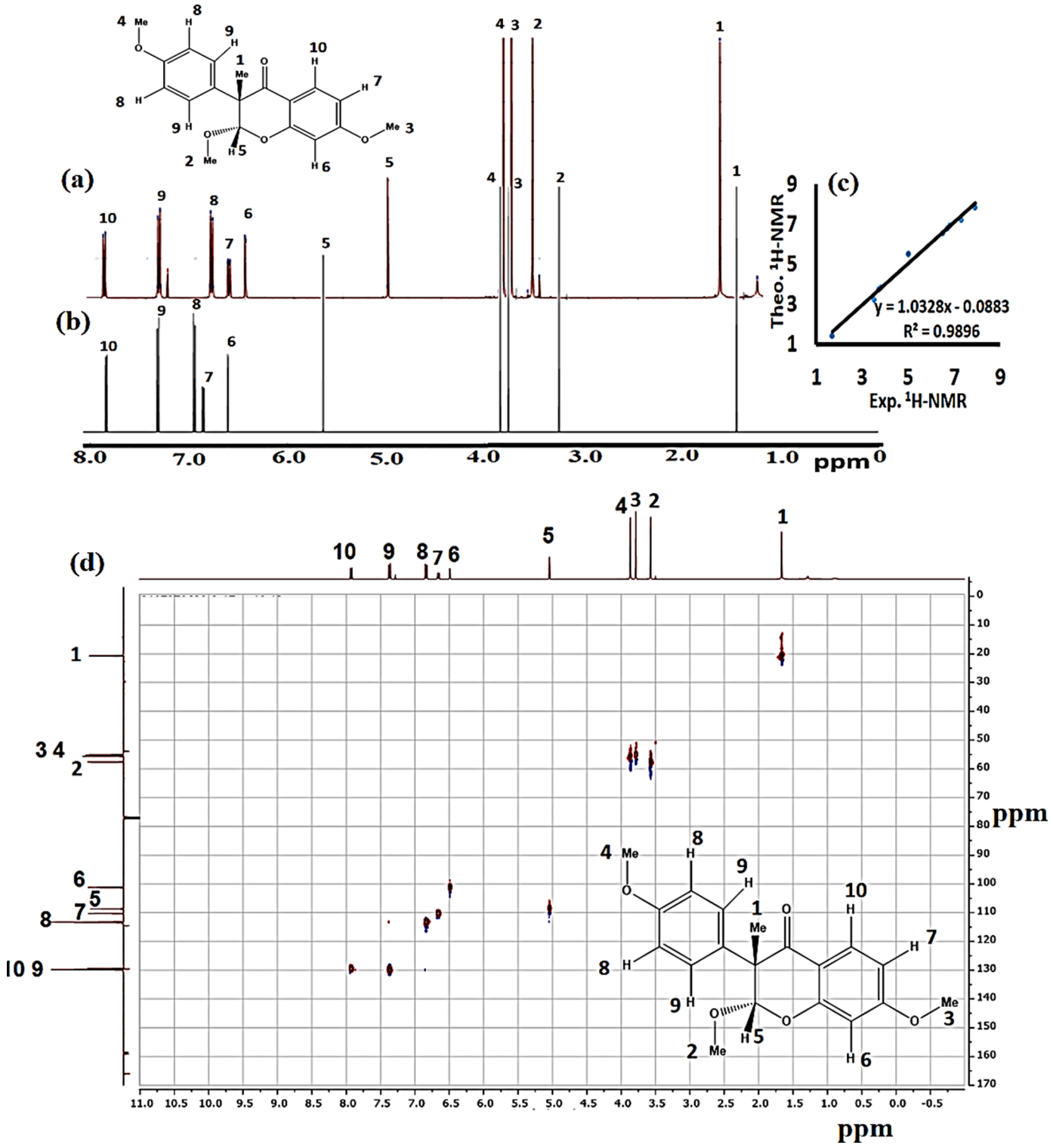

Fig. 5. (a) Exp., (b) Theo. ^{1}HNMR , (c) Exp./DFT-^{1}HNMR correlation, and (d) H—C NOSY.

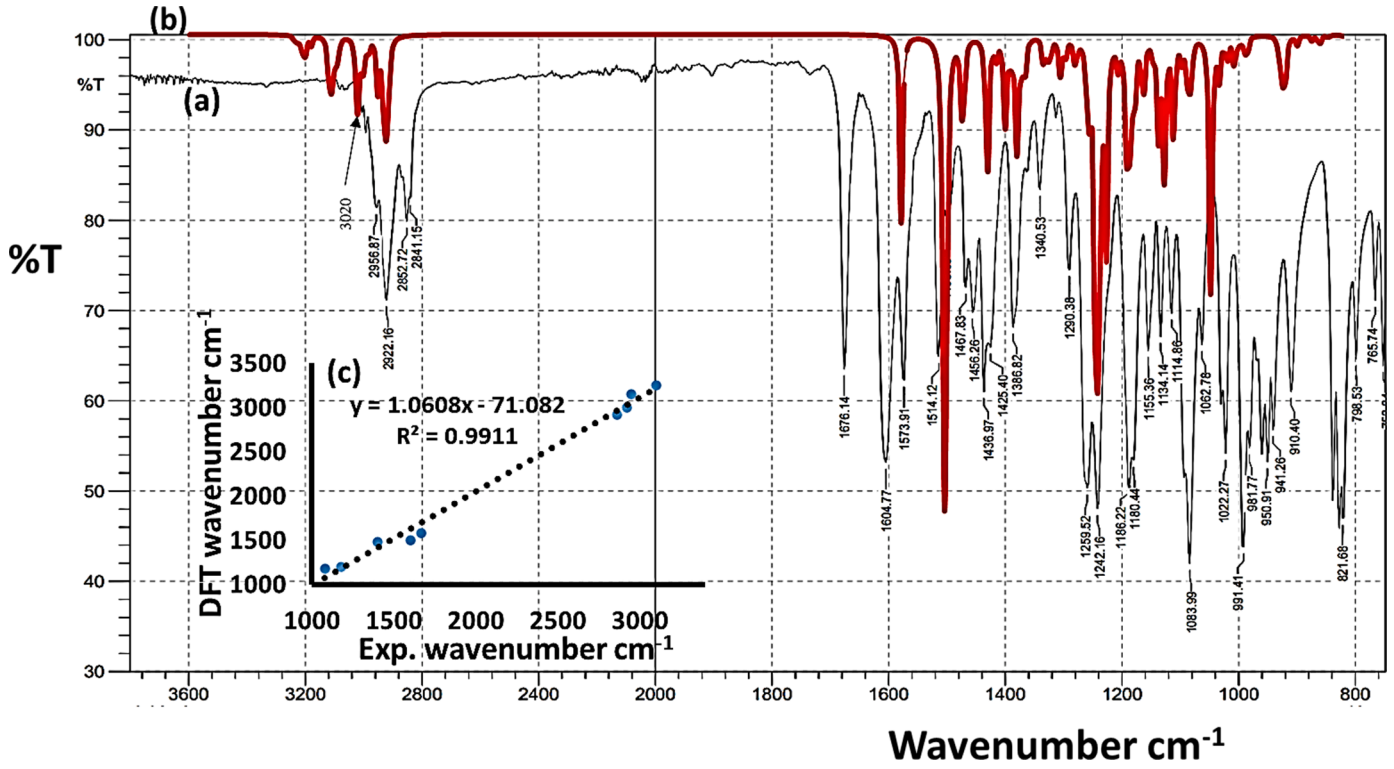

Fig. 6. (a) Exp. FT-IR, (b) theor. B3LYP-IR, and (c) Exp./DFT-IR graphical correlation.

3.6. FT-IR investigations

Fig. 6 depicts the FT/DFT-IR spectrum for 2,7-dimethoxy-3-(4-metho-xyphenyl)−3-methylchroman-4-one in the range of 4000–800 cm^{-1}, as well as its graphical correlation. Principal functional group vibrations found in the experimental infrared spectroscopy were $C_{ph\text{-}H}$ at 3020 cm^{-1}, $C_{alky\text{-}H}$ at 2950–2840 cm^{-1}, and C = O at 1676 cm^{-1}; all other functional groups were referred to their expected wavenumber regions (Fig. 6a). The DFT-theoretical IR measurements likewise revealed these functional groups, albeit with a little variance in chemical shifts (Fig. 6b), which is to be expected given that the theoretical measurements were conducted in the gaseous state and the practical observations in the solid state. Fig. 6c demonstrates that despite this, the graphical correlation is close to unity (0.9911).

3.7. LUMO/HOMO, TD-SCF/UV–vis., DOS and Tauc's optical gap analysis

The LUMO/HOMO B3LYP frontier orbitals and density of state (DOS) energy estimates are shown in Fig. 7. The $\Delta E_{HOMO/LUMO}$ found to be 4.501 eV (Fig. 7a). The energies of DOS [29] for LUMO/HOMO ΔE_{DOS} found to be 4.462 eV (Fig. 7b). The degree of convergence between the two techniques of calculating HOMOLUMO energy was high, with the difference between them not exceeding 0.039 eV. Moreover, the experimental UV–vis and TD-DFT/B3LYP analyses were compared in DMSO to comprehend the optical and detect the electronic characteristics. The UV–vis spectrum shows the existence of two absorption peaks at max 208 nm and 274 nm, which are attributable to π to π* electron transfer (Fig. 7c).

Similarly, TD-DFT/B3LYP calculations revealed two broadband at λ_{max} at 213 nm assigned to H-4=>L + 1(20%), H-2=>L + 1(68%) with $\Delta\lambda$= 5 nm with regard to the experimental band, and λ_{max} at 277 nm attributed to H-3=>LUMO(19%), H-1=>LUMO(74%) with $\Delta\lambda$= 3 nm with respect to the experimental band (Table 4). Moreover, Table 4 depicts the first 20 TD-DFT calculation bands with f>0.01, computed energy (cm^{-1}), wavelength (nm), and transition oscillator intensity (f).

The absence of visible absorption and the presence of only UV activities validate the compound's suitability as a photonic and optical material; hence, the experimental direct optical band gap for Tauc was developed, as depicted in Fig. 7d [30]. The Tauc's ΔE_g reflected the molecule at 4.18 eV, which is less than the predicted $\Delta E_{HOMO/LUMO}$ and ΔE_{DOS} but remains in high agreement. The TD-DFT of (2S,3S)−2,7-dimethoxy-3-(4-metho-xyphenyl)−3-methylchroman-4-one finding provided significant insight not only into electrical behavior, but also into the compatibility of experimental and computational spectra.

4. Conclusion

The novel 2,7-dimethoxy-3-(4-metho-xyphenyl)−3-methylchroman-4-one **2** was synthesized in a one-pot procedure by reacting 7,4′-dimethoxydaidzein **1** with sodium methoxide, followed by iodomethane. The XRD/DFT analysis validated the formation of a racemic compound; it emerged that the theoretical and experimental structural characteristics are very comparable. Due to the presence of four oxygen atoms in the molecule's backbone, a number of short CH⋯O hydrogen bonds were formed. The theoretical B3LYP-IR, TD-DFT, and ^{1}HNMR results correlated very well with the experimental FT-IR, UV–vis, and ^{1}HNMR results, respectively. Moreover, the actual Tauc optical observations were

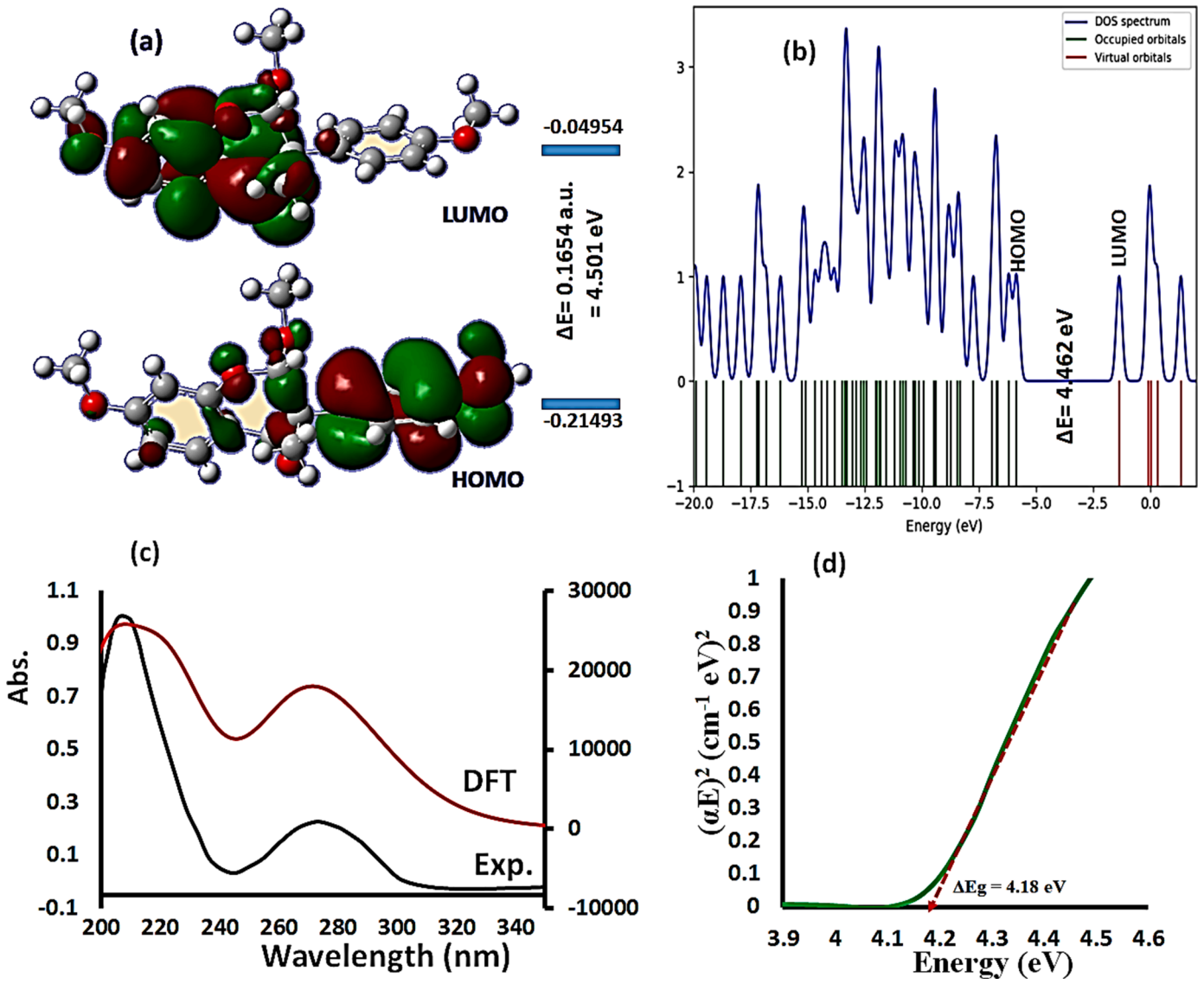

Fig. 7. (a) LUMO/HOMO energy and shape, (b) DOS, (c) UV–vis/TD-DFT, and (d) Tauc's direct optical gap diagrams.

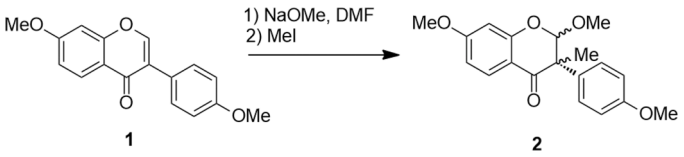

Scheme 1. Synthesis of **(±)**−2,7-dimethoxy-3-(4-metho-xyphenyl)−3-methyl-chroman-4-one.

validated by HOMO/LUMO and DOS calculations, while the energy predictions using EDOS and $E_{HOMO/LUMO}$ exhibited 0.28 and 0.32 eV discrepancies, respectively. In the experimental XRD-packing molecular lattice, the MEP, MAC/NBA, and HSA computations verified the electrostatic behavior of functional groups with many [H⋯⋯O] interactions.

CRediT authorship contribution statement

Nawaf Al-Maharik: Conceptualization, Methodology. **Malak Daqqa:** Data curation, Writing – review & editing. **Abeer AlObaid:** Data curation, Visualization. **Abdelkader Zarrouk:** Methodology, Software. **Ismail Warad:** Formal analysis, Writing – original draft.

Declaration of Competing Interest

The authors declare that they have no conflicts of interest.

Data availability

No data was used for the research described in the article.

Table 4
TD-DFT bands of 2,7-dimethoxy-3-(4-metho-xyphenyl)−3-methylchroman-4-one.

No.	E (cm^{-1})	λ (nm)	Osc. Str. (f)	Major Contribs
1	31332.2	319.2	0.0121	HOMO->LUMO (95%)
2	31877.5	313.7	0.0105	H-4->LUMO (24%), H-2->LUMO (68%)
3	35282.7	277.4	0.1907	H-3->LUMO (19%), H-1->LUMO (74%)
4	38162.9	262	0.3168	H-3->LUMO (67%), H-1->LUMO (21%)
5	39442.1	253.5	0.0142	H-4->LUMO (69%), H-2->LUMO (26%)
6	41342.4	241.9	0.0337	HOMO->L+2 (70%)
7	42991	232.6	0.0445	HOMO->L+1 (89%)
8	44783.1	223.3	0.1409	H-5->LUMO (33%), H-1->L+1 (52%)
9	45497.7	219.8	0.0741	H-5->LUMO (64%), H-1->L+1 (24%)
10	46289.8	216	0.0145	H-1->L+2 (94%)
11	46600.3	214.6	0.2388	HOMO->L+3 (71%)
12	46873.7	213.3	0.0109	H-4->L+1 (20%), H-2->L+1 (68%)
13	48412.6	206.6	0.019	H-2->L+2 (15%), H-1->L+3 (80%)
14	48551.4	206	0.081	H-4->L+2 (25%), H-2->L+2 (47%), H-1->L+3 (17%)
15	49808	200.8	0.0357	H-8->LUMO (13%), H-6->LUMO (71%)
16	50427.4	198.3	0.1197	H-4->L+3 (14%), H-3->L+1 (18%), H-2->L+3 (47%)
17	50562.9	197.8	0.1405	H-4->L+3 (11%), H-3->L+1 (40%), H-2->L+3 (22%)
18	50875	196.6	0.0011	H-4->L+1 (33%), H-3->L+2 (54%)
19	51204.9	195.3	0.1058	H-7->LUMO (13%), H-4->L+1 (33%), H-3->L+2 (19%)
20	52244.6	191.4	0.1102	H-7->LUMO (68%), H-3->L+1 (10%)

Acknowledgments

The authors extend their appreciation to the Researchers Supporting Project number (RSP2023R381), King Saud University, Riyadh, Saudi Arabia.

References

[1] N. Al-Maharik, Nat. Prod. Rep. 36 (2019) 1156–1195.
[2] S.I. Sohn, S. Pandian, Y.J. Oh, H.J. Kang, W.S. Cho, Y.S. Cho, Front. Plant Sci. 12 (2021), 670103.
[3] C. Rípodas, V. Dalla, O.M. Aguilar, M.E. Zanetti, F.A. Blanco, Plant Physiol. Biochem. 68 (2013) 81–89.
[4] O. Kraszewska, A. Nynca, B. Kaminska, R. C., Fitoestrogeny Postêpy Biol. Komórki 1 (2007) 189–205.
[5] M.J. Messi3na, C.E. Wood, Nutr. J. 7 (2008) 17–28.
[6] M. Pabich, M. Materska, Nutrients 11 (2019) 1660–1671.
[7] H.M. Abdelrazek, M.M. Mahmoud, H.M. Tag, S.M. Greish, D.A. Eltamany, M. T. Soliman, Oxid. Med. Cell Longev. 10 (2019) 1–13.
[8] G.-A. Yoon, S. Park, Nutr. Res. Pract. 8 (2014) 618–624.
[9] S. Bellou, E. Karali, E. Bagli, N. Al-Maharik, L. Morbidelli, M. Ziche, H. Adlercreutz, C. Murphy, T. Fotsis, Mol. Cancer 11 (2012) 35–44.
[10] O. Kucuk, Cancer 123 (2017) 1901–1903.
[11] E.J. Choi, G.-H. Kim, Mol. Med. Rep. 7 (2013) 781–784.
[12] X. Zheng, S.K. Lee, O. K, J. Med. Food 19 (2016) 1–14.
[13] E. Miadoková, Interdiscip. Toxicol. 2 (2009) 211–218.
[14] A. Zarrouk, I. El Ouali, M. Bouachrine, B. Hammouti, Y. Ramli, E. Essassi, I. Warad, A. Aouniti, R. Salghi, Res. Chem. Intermed. 39 (2013) 1125–1133.
[15] M. Rbaa, F. Benhiba, M. Galai, S. Abousalem, M. Ouakki, C. Lai, B. Lakhrissi, C. Jama, I. Warad, M.Ebn Touhami, A. Zarrouk, Chem. Phys. Lett. 754 (2020) 137771–137779.
[16] I. Badran, S. Tighadouini, S. Radi, A. Zarrouk, I. Warad, J. Mol. Struct. 1229 (2021) 129799–129807.
[17] M. J. Frisch, G. W. Trucks, H. B. Schlegel, G. E. Scuseria, M. A. Robb, J. R. Cheeseman, G. Scalmani, V. Barone, B. Mennucci, G. A. Petersson, H. Nakatsuji, M. Caricato, X. Li, H. P. Hratchian, A. F. Izmaylov, J. Bloino, G. Zheng, J. L. Sonnenberg, M. Hada, M. Ehara, K. Toyota, R. Fukuda, J. Hasegawa, M. Ishida, T. Nakajima, Y. Honda, O. Kitao, H. Nakai, T. Vreven, J. A. Montgomery, Jr., J. E. Peralta, F. Ogliaro, M. Bearpark, J. J. Heyd, E. Brothers, K. N. Kudin, V. N. Staroverov, R. Kobayashi, J. Normand, K. Raghavachari, A. Rendell, J. C. Burant, S. S. Iyengar, J. Tomasi, M. Cossi, N. Rega, J. M. Millam, M. Klene, J. E. Knox, J. B. Cross, V. Bakken, C. Adamo, J. Jaramillo, R. Gomperts, R. E. Stratmann, O. Yazyev, A. J. Austin, R. Cammi, C. Pomelli, J. W. Ochterski, R. L. Martin, K. Morokuma, V. G. Zakrzewski, G. A. Voth, P. Salvador, J. J. Dannenberg, S. Dapprich, A. D. Daniels, Ö. Farkas, J. B. Foresman, J. V. Ortiz, J. Cioslowski, and D. J. Fox, Gaussian 09W, Gaussian Inc., Wallingford CT, 2009.
[18] S.K. Wolff, D.J. Grimwood, J.J. McKinnon, M.J. Turner, D. Jayatilaka, M. A. Spackman, Crystal Explorer 3.0, University of Western Australia, Perth, 2012.
[19] Bruker APEX2 and SAINT, Bruker AXS Inc., Madison, Wisconsin, 2007.
[20] G.M. Sheldrick, Acta Crystallogr. Sect. A 64 (2008) 112–122.
[21] A.N. Kochetov, L.A. Nosikova, L.G. Kuzmina, Cryst. Rep. 65 (2020) 721–725.
[22] I. Brito, J. Bórquez, M. Simirgiotis, A. Cárdenas, Z. Kristallogr. 233 (2018) 61–64.
[23] S.Y. Shin, M. Yoo and D. Koh, Z. Kristallogr. NCS, 235 (20202) 1253–1255.
[24] F. Abu Saleemh, S. Musameh, A. Sawafta, P. Brandao, C.J. Tavares, S. Ferdov, A. Barakat, A. Al Ali, M. Al-Noaimi, I. Warad, Arab. J. Chem. 10 (2017) 845–854.
[25] Ö. Tamer, N. Dege, G. Demirtaş, D. Avcı, Y. Atalay, M. Macit, S. Şahin, J. Mol. Struct. 1063 (2014) 295–306.
[26] M.R. Albayati, S. Kansız, N. Dege, S. Kaya, R. Marzouki, H. Lgaz, R. Salghi, I.H. Ali, M.M. Alghamdi, I.-M. Chung, J. Mol. Struct. 1205 (2020), 127654.
[27] N. Dege, H. Gokce, O.E. Dogan, G. Alpaslan, T. Agar, S. Muthu, Y. Sertf, Colloids Surf. A Physicochem. Eng. Asp. 638 (2022) 128311–128325.
[28] N. Dege, N. Şenyüz, H. Batı, N. Günay, D. Avcı, Ö. Tamer, Y. Atalay, Spectrochim. Acta A Mol. Biomol. Spectrosc. 120 (2014) 323–331.
[29] S. Demir, F. Tinmaz, N. Dege, I. Ilhan, J. Mol. Struct. 1108 (2016) 637–648.
[30] J. Tauc, R. Grigorovici, A. Vancu, Phys. Status Sol. B 152 (1966) 627–637.